Grant-Free Random Access With Backscattering Self-Conjugating Metasurfaces

Davide Dardari, *Senior Member, IEEE*, Marina Lotti, *Graduate Student Member, IEEE*, Nicolò Decarli, *Member, IEEE*, and Gianni Pasolini, *Member, IEEE*

***Abstract*—Recently, grant-free random access (GFRA) schemes have received significant attention by the research community as a solution for extremely low-latency and short packet transmissions in new industrial Internet-of-Things and digital twins applications. However, implementing such schemes in the mmWave and THz frequency bands is challenging due to the need for multiple-input multiple-output (MIMO) links to counteract the high path loss and provide sufficient spatial filtering. This results in unacceptable signaling overhead for channel estimation, slow beam alignment procedures between the access point (AP) and the sensors, as well as high sensor complexity and energy consumption. In this paper, we propose the adoption of a self-conjugating metasurface (SCM) at the sensor side, where the signal sent by the AP is backscattered after being conjugated and phase-modulated according to the data to be transmitted by the sensor. We introduce a novel SCM-based GFRA protocol enabling the detection of new sensors and the establishment of parallel MIMO uplink communications with extremely low latency. This is achieved in a blind manner, eliminating the need for radiofrequency chains and digital processing at the sensor side, as well as explicit channel estimation and time-consuming beam alignment schemes.**

***Index Terms*—Self-conjugating metasurfaces, grant-free random access, retro-directive backscattering, MIMO, fast beamforming.**

I. Introduction

FUTURE wireless networks are anticipated to meet very challenging requirements in terms of data rate, latency, energy efficiency, and node density, in order to enhance the performance of existing massive Machine Type Communication (mMTC) applications and enable new ones [1]. Among them, the creation of digital twin worlds perfectly intertwined with physical objects in industrial Internet-of-Things (IIoT) environments is certainly one of the most challenging [2], [3]. In this context, there is a simultaneous need to meet several demanding requirements, such as ultra-low latency ($< 100\,\mu$s), low jitter ($\approx 1-2\,\mu$s), ultra-massive access ($10^7 \text{sensors}/\text{km}^2$), high energy efficiency, and low complexity. In addition, in mMTCs, the generated traffic is often sporadic and random, characterized by the transmission of short packets that can be as small as 32 bytes.

Under such circumstances, in order to maintain access latency at extremely low levels, coordination actions by the access point (AP), such as scheduling, synchronization, or retransmission, are generally avoided in favor of grant-free random access (GFRA) schemes, where sensors start transmitting as long as they have a new packet ready [4]. Therefore, GFRA schemes must address not only the challenges of detecting active sensors and estimating the channel but also the issue of inter-sensor interference caused by collisions [5], [6]. In this regard, sensors are typically assigned different preambles (or pilots) for their packets. However, to minimize overhead, preambles are often reused, which means collisions can still occur. Various solutions have been proposed to cope with these effects. For instance, coded random access protocols allow an increased level of reliability thanks to the joint exploitation of interference cancelation and coding techniques on top of classical ALOHA-based random-access protocols [7]. Explicit preamble transmission is avoided in the coded random-access scheme investigated in [8] by assigning to each sensor a unique channel access pattern which is used to embed sensor identities and facilitate the detection. In any case, coded random access relies on transmitting multiple replicas of the same packet to enable interference cancellation, which can potentially hinder the attainment of sub-ms latency.

It is also worth noting that most GFRA schemes employ single antenna sensors with a single-radiofrequency (RF) chain. A multi-antenna AP, i.e., an uplink single-input multiple-output (SIMO) configuration, has demonstrated the capability of reducing the effect of inter-sensor interference to any level provided that the number of antennas at the AP grows indefinitely under typical channel characteristics. In [5], an asymptotic regime analysis of sensor activity detection and channel estimation is carried out as the number of antennas at the AP becomes massive. Specifically, the authors quantify the performance of sensor activity detection and channel estimation when randomly generated non-orthogonal pilot

Received 15 February 2024; revised 12 June 2024; accepted 12 August 2024. Date of publication 9 September 2024; date of current version 8 October 2024. This work was partially supported by the European Union under the Italian National Recovery and Resilience Plan (NRRP) of NextGenerationEU, partnership on "Telecommunications of the Future" (PE00000001 - program "RESTART"), and in part by the HORIZON-JU-SNS-2022-STREAM-B-01-03 6G-SHINE Project under Grant 101095738. The associate editor coordinating the review of this article and approving it for publication was Z. Chang. *(Corresponding author: Nicolò Decarli.)*

Davide Dardari, Marina Lotti, and Gianni Pasolini are with the Dipartimento di Ingegneria dell'Energia Elettrica e dell'Informazione "Guglielmo Marconi", University of Bologna, 47521 Cesena, Italy, and also with the WiLab, CNIT, 40133 Bologna, Italy (e-mail: davide.dardari@unibo.it; marina.lotti2@unibo.it; gianni.pasolini@unibo.it).

Nicolò Decarli is with the National Research Council, Institute of Electronics, Computer and Telecommunication Engineering, 00185 Rome, Italy, and also with the WiLab, CNIT, 40133 Bologna, Italy (e-mail: nicolo.decarli@cnr.it).

Digital Object Identifier 10.1109/TCCN.2024.3449648

sequences are assigned to each device. They show that the error in sensor activity detection can be reduced to any desired degree by increasing the number of antennas, whereas the channel estimation error and the overhead for pilots remain the main bottleneck. It is worth highlighting that in typical multi-antenna GFRA schemes, such as the works [6], [9], [10], [11], the term "massive multiple-input multiple-output (MIMO)" pertains to the number of antenna elements of the AP although sensors are single antenna, i.e., they are actually SIMO. An alternative approach to avoid the preamble collision involves the adoption of grant-free non-orthogonal multiple access (NOMA) schemes, which have demonstrated superior performance compared to traditional random-access methods. To address interference among users (e.g., instances where two users utilize the same identification code or preamble), physical radio resources can be scaled by associating data symbols with a signature, typically presented in the form of spreading sequences, power levels, pilot sequences, codebooks, interleavers, or patterns, [12], [13], [14]. However, to the best of the author's knowledge, all the papers that exploit NOMA in the literature utilize SIMO schemes, without overcoming the path loss problem due to high frequency, and most of them employ slotted-ALOHA protocols, which require synchronization.

Looking ahead, the exploitation of high frequencies in the mmWave and THz bands is under consideration for IIoT communications [15], [16], [17], [18], which however requires massive antenna arrays with very narrow beams also at the sensor side, i.e., a true MIMO scheme, to compensate for the high path loss and obtain better spatial filtering to reduce the interference between sensors that are using the same radio resource. Additionally, the better angular discrimination allows for improved security, since a malicious user cannot detect the presence of the sensor-AP communication signal outside the area illuminated by their sharp beam itself. However, the utilization of MIMO brings forth additional issues. For instance, channel state information (CSI) estimation becomes extremely challenging. Typically, it relies on the assumption that devices remain active for a long period, allowing for the allocation of long preambles without a significant loss in efficiency. Conversely, in GFRA, the CSI has to be estimated with an extremely limited preamble. Moreover, the initial beam alignment procedure requires both the AP and sensor to test all possible pairs of angles before the sensor becomes visible to the AP and the communication established [19]. However, this is in contrast with the uncoordinated nature of GFRA. These approaches either involve some computational effort on both sides, which affects sensor hardware complexity and power consumption, or long training data/search time, which increases latency. Clearly, these problems are emphasized when the number of antennas is high, as can happen when considering high frequencies, such as sub-THz/THz, where also technological constraints place several limitations on the flexibility in processing the signal sent/received by each antenna element (digital bottleneck). Therefore, it is of paramount importance to study solutions enabling ultra-low latency MIMO GFRA using low-complexity, low-power devices at mmWave and beyond, characterized by minimal or no overhead associated with CSI estimation and sensor detection.

To lower the complexity and energy consumption, backscattering communication solutions (in the following, *BackCom*) have recently attracted some interest. Among the different backscattering techniques, reconfigurable metasurfaces can be adopted to embed information from attached sensors while reflecting a signal emitted by the AP [20], [21], [22]. This is done through the adoption of backscatter modulation, so that they can be seen as a generalization of radio frequency identification (RFID) systems [23], [24]. BackCom metasurfaces are semi-passive devices, making them energy efficient. However, they require reconfiguration each time the channel changes, necessitating complex CSI estimation procedures. These procedures are further complicated by the cascade nature of the channel. Additionally, a dedicated control link is needed, leading to associated overhead and latency. As a consequence, BackCom solutions appear to be more suitable for applications with fixed sensors and periodic traffic and not for GFRA in uncoordinated dynamic scenarios.

Despite the rich literature on the subject, to the authors' knowledge, no solutions have been proposed ensuring a true MIMO GFRA with ultra-low latency (e.g., $< 100\,\mu$s) and jitter, no overhead for CSI estimation, in a mMTC scenario using ultra-low complexity devices. The main question is therefore whether it is possible to exploit the backscattering technology to enable MIMO GFRA schemes with the above-mentioned characteristics.

A. Our Contribution

In this paper, we introduce a novel scheme that overcomes previous limitations, enabling extremely low latency GFRA for asynchronous low-complexity MIMO devices working in backscattering. For the purposes of this paper, we focus on a specific type of reconfigurable metasurface, referred to as self-conjugating metasurface (SCM). SCMs possess the capability of reflecting an electromagnetic (EM) wave with a complex envelope that is the conjugate of the impinging EM wave's envelope, resulting in the retrodirectivity effect [25]. Retrodirectivity has been investigated in different contexts such as radar, wireless power transfer, collision avoidance systems, microwave imaging or detection, RFID systems, and remote information retrieval from sensors. However, to the authors' best knowledge, its use for efficient wireless communications has been little studied [25] and has never been considered for GFRA MIMO systems, as we do in this work. In particular, in this paper we build on our previous work [26], where a modulating SCM was proposed to jointly communicate and perform beam tracking with always active sensors in a fast time-variant channel. Our goal now is to advance this work by designing a GFRA MIMO scheme with asynchronous sensors exploiting the properties of SCMs. One important peculiarity of the proposed scheme is that it does not need any overhead for CSI estimation or any RF chain/Digital-to-Analog converter (DAC) and baseband signal processing at the sensor side, thus allowing the efficient transmission of short packets in mMTC applications with low-complexity devices.

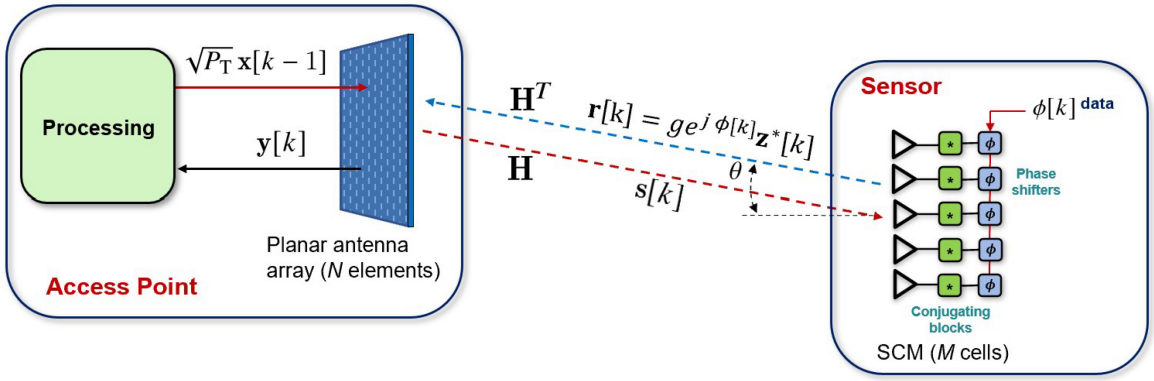

Fig. 1. Principle scheme of a modulating self-conjugating metasurface (SCM)-based MIMO communication.

Specifically, the main concept entails implementing multiple parallel tasks at the AP, aimed at transmitting appropriate interrogation signals and processing the sensors' responses received by the AP's antenna array. More precisely, in order to detect new sensors willing to transmit data, a dedicated *Scouting Task* is always running at the AP, which transmits interrogation signals searching for sensors on a channel subspace orthogonal to those used by already active links. On the other side of the link, sensors with data queued for transmission react by backscattering the interrogation signal towards the AP, leveraging the retrodirectivity property enabled by their SCM, while simultaneously modulating it with their own data. It will be shown that by operating in this manner, the AP can derive the beamforming vectors and establish a true MIMO uplink communication with sensors in a blind and nearly optimal way, eliminating the need for either CSI estimation or time-consuming beam alignment schemes, and hence without any computational effort at the sensor side. The AP can also extract the sensor's identification from the signals received from the SCMs. Essentially, the sensor engaged in backscattering the incoming signal using the SCM could incorporate its ID into the reflected signal. Whenever a new sensor is detected, the AP initiates a dedicated task, named *Communication Task*, that utilizes the beamforming vector estimated by the Scouting Task to decode the sensor data. The result is a scheme where complexity grows linearly with the number of sensors and is capable of managing asynchronous random transmissions of packets of any size without the explicit estimation of the multi-sensor MIMO channel, thus ensuring an almost zero latency and no jitter independently of the number of sensors. We further characterize analytically the convergence behavior of the Scouting Task taking into account the noise generated by the SCM and the AP. Numerical results reveal that optimal beamforming, and hence beam alignment, can be achieved within a few symbol times, without any processing at the sensor. It is important to emphasize that the increased path loss due to the backscatter nature of the communication link can be easily compensated by increasing the number of antennas at the sensor.

The main novelty and differences with respect to current GFRA and BackCom schemes are: *i)* our scheme exploits the gain of a MIMO link as it is a true MIMO (not SIMO) GFRA solution; *ii)* contrarily to BackCom schemes, it does not require any dedicated control channel and CSI estimation to reconfigure the metasurface; *iii)* it does not suffer from the trade-off between preamble overhead and preamble collision, as no preambles are needed in this case, unlike the baseline GFRA approach; *iv)* the adoption of the SCM allows an extremely low-complexity and low-power design of the sensor because no DAC/RF-chains are needed; *v)* our scheme is not alternative to NOMA-based GFRA. Instead, NOMA can be added on top of our scheme to further increase its performance; *vi)* as will be shown, our scheme is particularly well-suited for use in high-frequency bands such as mmWave and THz.

The rest of the paper is structured as follows: in Section II, a brief overview of SCMs is given and the strategy to exploit them to transmit data is proposed. The illustration of the working principle of SCM-based communications is given in Section III. The proposed algorithm for GFRA is described in Section IV and the convergence analysis is presented in Section V. Numerical results are illustrated in Section VI, whereas some further remarks and comparisons with other baseline GFRA, NOMA-based GFRA, and BackCom schemes are addressed in Section VII. The conclusions are drawn in Section VIII.

B. Notation and Definitions

Boldface lower-case letters are vectors (e.g., $\mathbf{x}$), whereas boldface capital letters are matrices (e.g., $\mathbf{H}$), where $\mathbf{I}_N$ is the identity matrix of size N, $\|\mathbf{x}\|$ represents the Euclidean norm of vector $\mathbf{x}$ and $\mathbf{x}^*$ is its conjugate. $\mathbf{H}^*$, $\mathbf{H}^T$ and $\mathbf{H}^\dagger$ indicate, respectively, the conjugate, the transpose and the conjugate transpose operators applied to matrix $\mathbf{H}$, whereas $\|\mathbf{H}\|_{\mathrm{F}}$ denotes the Frobenius norm of $\mathbf{H}$. The notation $x \sim \mathcal{CN}(m, \sigma^2)$ indicates a complex circular symmetric Gaussian random variable (RV) with mean m and variance σ^2, whereas $\mathbf{x} \sim \mathcal{CN}(\mathbf{m}, \mathbf{C})$ denotes a complex Gaussian random vector with mean $\mathbf{m}$ and covariance matrix $\mathbf{C}$.

II. Modulating Self-Conjugating Metasurfaces

With reference to the sensor's side of Fig. 1, consider a SCM (or an antenna array) composed of M elements, namely cells (or antennas) and a narrowband impinging signal $\mathbf{s}[k] = [s_1[k], s_2[k], \ldots, s_M[k]]^T$ of bandwidth W, where $s_m[k]$ represents the equivalent low-pass discrete-time version

of the signal at the input of the m-th cell at discrete time k. As previously mentioned, an SCM is characterized by the property such that the backscattered low-pass equivalent signal is the conjugate of the input low-pass equivalent signal [25], that is,

$$\mathbf{r}[k] = g\,\mathbf{s}^*[k] + g\,\boldsymbol{\eta}^*[k] \tag{1}$$

where $\boldsymbol{\eta}[k] \in \mathbb{C}^{M\times 1}$ is the additive white Gaussian noise (AWGN), with $\boldsymbol{\eta}[k] \sim \mathcal{CN}(\mathbf{0}, \sigma_\eta^2 \mathbf{I}_M)$, and g is the gain of the cell ($g < 1$ if it is passive). Note that $\sigma_\eta^2 = \kappa T_0 F_{\mathrm{SCM}}\, W$, being κ the Boltzmann constant, $T_0 = 290\,\mathrm{K}$, and F_{SCM} the cell's noise figure [27], [28]

The fundamental property exhibited by SCMs is *retrodirectivity* [25]. Specifically, when an SCM is illuminated by a plane wave with an incident angle θ, the signal is ideally backscattered in the same direction, towards the signal source (see Fig. 1). For example, if a uniform linear array (ULA)-like SCM with inter-element spacing Δ is considered, an impinging plane wave with incident angle θ can be generically expressed as $s_m[k] = A\, e^{\jmath \frac{2\pi}{\lambda} m\,\Delta\,\sin(\theta)}$, for $m = 1, 2, \ldots, M$, where λ is the wavelength and A is a generic complex constant. According to (1), the corresponding backscattered signal is $g\, s_m^*[k] = g\, A^*\, e^{\jmath \frac{2\pi}{\lambda} m\,\Delta\,\sin(-\theta)}$, for $m = 1, 2, \ldots, M$, which originates a plane wave reflected back toward the same direction θ. Clearly, the presence of the noise contribution that appears in (1) impacts the system's performance, as will be discussed in the numerical results of Section VI.

The most common approach to realize the self-conjugating property is through heterodyne mixing of the incoming wave, centred at frequency f_0, with a locally generated sinusoid oscillating at $2f_0$ [25], [29]. While heterodyne mixing arrays necessitate active components, passive retrodirectivity can be obtained using a Van Atta array [30], making it more suitable for implementation in very low-cost and energy efficient solutions. A Van Atta array comprises antenna elements arranged in symmetrical pairs and connected through transmission lines. The elements are deployed in a mirror-symmetric manner to induce an equivalent phase-conjugation effect for the reflected wave compared to the incident wave. Recent developments have demonstrated that metasurfaces can also be designed to provide passive retrodirectivity. This property is achieved by engineering the surface impedance based on a supercell design periodicity greater than the wavelength [31]. By abstracting from the specific implementation technology (antenna array or metasurface), hereinafter we will denote retrodirective devices as SCMs.

Suppose, now, that the SCM not only performs the conjugation and (possible) amplification of the received signal but also introduces, in each k-th symbol interval, a phase shift $\phi[k]$, same for all cells, that incorporates the information to be transmitted by the sensor in that interval (see Fig. 1). The phase shift can be implemented in a similar way as in RFIDs, where typically a PIN diode, a varactor or a RF switch is added at the load of each cell [32]. As a consequence, the vector of the backscattered signal becomes

$$\mathbf{r}[k] = g\, e^{\jmath\phi[k]}\, \mathbf{z}^*[k] \tag{2}$$

where $\mathbf{z}[k] = \mathbf{s}[k] + \boldsymbol{\eta}[k]$. The conjugation operation, which enables the retrodirectivity property, serves as the foundation for the algorithm proposed in the following sections. Since the phase $\phi[k]$ affects all cells of the metasurface, it does not compromise the retrodirectivity behavior as the common phase term can be absorbed by the constant A. Moreover, the implementation of the modulating SCM does not require DAC/RF chains as data directly modulates the phase sequence $\{\phi[k]\}$, thus allowing a low-cost, low-complexity, low-energy consumption multi-antenna sensor.

III. Working Principle of SCM-Based MIMO Communication

In this section, we start with the single-sensor uplink scenario, shown in Fig. 1, with the purpose to illustrate how data can be transmitted from an SCM-based sensor to the AP. In particular, we consider an AP, equipped with an antenna array of N elements, capable of full-duplex narrow-band transmission with bandwidth W. The time interval T between time instants $k-1$ and k is in the order of $1/W$.[1] The sensor is realized according to the scheme described in Section II, thus incorporating an SCM composed of M cells. Let $\sqrt{P_{\mathrm{T}}}\,\mathbf{x}[k-1] \in \mathbb{C}^{N\times 1}$ be the vector containing the signal transmitted by the N elements of the AP's antenna array during the k-th time interval $[(k-1)\,T, k\,T]$, where P_{T} is the transmitted power and $\mathbf{x}[k-1]$ is a unitary norm beamforming vector, i.e., the precoding vector designed to steer the beam toward the sensor according to the scheme proposed in Section IV. The transmitted signal is received, modulated and retro-directed by the sensor during the time interval k, then collected by the AP. Here, we assume symbol-level synchronization between the sensor and the AP.[2] Specifically, the signal received by the sensor in the k-th time interval is

$$\mathbf{z}[k] = \mathbf{s}[k] + \boldsymbol{\eta}[k] = \sqrt{P_{\mathrm{T}}}\,\mathbf{H}\,\mathbf{x}[k-1] + \boldsymbol{\eta}[k] \tag{3}$$

where $\mathbf{H} \in \mathbb{C}^{M\times N}$ denotes the channel matrix. At the sensor, information data to be transmitted is associated with the phase sequence $\{\phi[k]\}_{k=1}^{K}$, forming a packet of length K symbols, according to any phase-based signaling scheme (e.g., binary phase-shift keying (BPSK)). Without loss of generality, we consider that all transmitted packets have the same length K, even though packets with different lengths can be easily managed by the scheme proposed in this paper without any change. The signal backscattered by the sensor, according to (2), is

$$\mathbf{r}[k] = g\, e^{\jmath\phi[k]}\,\mathbf{z}^*[k] = \sqrt{P_{\mathrm{T}}}\, g\, e^{\jmath\phi[k]}\,\mathbf{H}^*\,\mathbf{x}^*[k-1] + g\,\boldsymbol{\eta}^*[k] \tag{4}$$

being $\phi[k]$ the phase associated to the k-th data symbol of the transmitted packet. The same phase term should also multiply

[1] When describing the transmitted signal and the signal received/retro-directed by the sensor, time instants k should be intended as intervals. Sampling is operated at the AP after standard matched filter processing of the signal in the last symbol interval of duration T.

[2] The analysis of schemes at the AP capable of synchronizing with the local clock of the sensor is outside the scope of this paper. The interested reader is referred to [33] for comprehensive treatments on digital communication and synchronization techniques.

the noise component $\boldsymbol{\eta}$, but it is absorbed by the random phase of the noise, which is uniformly distributed in $[0, 2\pi)$. Hence, it can be ignored. At the AP side, the received signal at time k is

$$\mathbf{y}[k] = \sqrt{P_{\mathrm{T}}}\, g\, e^{\jmath\phi[k]}\, \mathbf{H}^T \mathbf{H}^* \mathbf{x}^*[k-1] + g\, \mathbf{H}^T\, \boldsymbol{\eta}^*[k] + \mathbf{w}[k] \tag{5}$$

where $\mathbf{w}[k] \sim \mathcal{CN}(\mathbf{0}, \sigma_w^2 \mathbf{I}_N)$ is the AWGN at the receiver, $\sigma_w^2 = \kappa T_0 F_{\mathrm{AP}}\, W$, being F_{AP} the AP's noise figure. The noise term $\mathbf{w}[k]$ might also include any clutter backscattered by the surrounding environment whose specific characterization depends on the environment itself. For further convenience, we can rewrite (5) as

$$\mathbf{y}[k] = \sqrt{P_{\mathrm{T}}}\, e^{\jmath\phi[k]}\, \mathbf{A}^*\, \mathbf{x}^*[k-1] + \mathbf{n}^*[k] \tag{6}$$

where we have defined $\mathbf{A} = g\, \mathbf{H}^\dagger \mathbf{H} \in \mathbb{C}^{N\times N}$ and $\mathbf{n}^*[k] = g\, \mathbf{H}^T\, \boldsymbol{\eta}^*[k] + \mathbf{w}[k] \sim \mathcal{CN}(\mathbf{0}, \sigma_w^2 \mathbf{I}_N + \sigma_{\boldsymbol{\eta}}^2 \mathbf{A}^*)$, which includes all the noise terms. Note that, because of the conjugation operated by the SCM, $\mathbf{A}$ is not the round-trip channel, which is given, instead, by $g\, \mathbf{H}^T \mathbf{H}$. For this reason, we refer to $\mathbf{A}$ as the *modified round-trip channel*. This is a fundamental characteristic for the proposed scheme to work properly as will be clear in the following.

Denote with λ_j the j-th eigenvalue of $\mathbf{A}$, where $\lambda_1 \geq \lambda_2 \geq \ldots, \geq \lambda_N$, and $\mathbf{v}_j$ is the corresponding eigenvector (direction). As a consequence, vector $\mathbf{n}[k]$ can be decomposed as

$$\mathbf{n}[k] = \sum_{j=1}^{N} n_j[k]\, \mathbf{v}_j \tag{7}$$

where $n_j[k]$ is the projection of $\mathbf{n}[k]$ onto the j-th direction $\mathbf{v}_j$, and $n_j \sim \mathcal{CN}(0, \sigma_j^2)$, with $\sigma_j^2 = \sigma_w^2 + \lambda_j\, \sigma_\eta^2$. In a typical practical setting, the modified round-trip channel gain $\|\mathbf{A}\|_{\mathrm{F}}^2$ is much less than one, then the noise component $\mathbf{w}[k]$ becomes the dominant term in $\mathbf{n}[k]$ and hence we can write with good approximation $\sigma_j^2 = \sigma^2$, $\forall j$, with $\sigma^2 \simeq \sigma_w^2$ (isotropic noise). Interestingly, thanks to the conjugating operation at the sensor's SCM, $\mathbf{A}$ is Hermitian, and its eigenvectors correspond to the left-eigenvectors of the MIMO channel $\mathbf{H}$. Therefore, the estimation of the optimum beamforming vector $\mathbf{x}[k]$ is equivalent to computing the top-eigenvector $\mathbf{v}_1$ of the modified round-trip channel $\mathbf{A}$ at the AP without requiring any processing at sensor side, as it will be clarified in Section IV.

Information data can be extracted by the AP at each time interval by forming the decision variable $u[k]$ through the correlation of the received vector $\mathbf{y}[k]$ with the complex conjugate of the beamforming vector $\mathbf{x}^\dagger[k-1]$, that is

$$u[k] = \mathbf{x}^\dagger[k-1]\, \mathbf{y}^*[k]. \tag{8}$$

In particular, assuming a perfect estimation of the beamforming vector $\mathbf{v}_1$ is available, then $\mathbf{x}[k-1] = \mathbf{v}_1$ and

$$\begin{aligned} u[k] &= \sqrt{P_{\mathrm{T}}}\, e^{-\jmath\phi[k]}\, \mathbf{v}_1^\dagger\, \mathbf{A}\, \mathbf{v}_1 + \mathbf{v}_1^\dagger\, \mathbf{n}[k] \\ &= \sqrt{P_{\mathrm{T}}}\, \lambda_1\, e^{-\jmath\phi[k]} + n_1[k] \end{aligned} \tag{9}$$

with $n_1 \sim \mathcal{CN}(0, \sigma^2)$. Starting from $u[k]$, a decision on the phase $\phi[k]$ can be made by taking its argument, i.e., $\hat{\phi}[k] = \mathrm{demodulation}(-\arg u[k])$, where $\mathrm{demodulation}(\cdot)$ is the data detection function which depends on the particular signaling scheme considered. Without loss of generality, our numerical results have been obtained considering the BPSK scheme. The corresponding signal-to-noise ratio (SNR) at the decision device is

$$\mathsf{SNR} = \frac{P_{\mathrm{T}}\, \lambda_1^2}{\sigma^2}. \tag{10}$$

It is worth noticing that when the channel has rank $r = \mathrm{rank}(\mathbf{H}) = 1$, the resulting communication scheme is capacity-optimal provided that an accurate estimation of the beamforming vector $\mathbf{v}_1$ is available. In fact, for $\mathrm{rank}(\mathbf{H}) = 1$, no multiplexing gain can be achieved. To maximize the capacity in this scenario, the optimal strategy is to exploit the beamforming gain by using a precoding vector that concentrates energy of the AP in the direction of the SCM, i.e., the top eigenvector $\mathbf{v}_1$. In a line-of-sight (LOS) channel, this results in a specific angular beam at the AP side. In the case of non-line-of-sight (NLOS) or multipath environments, the precoding vector ensures that the multipath components are received coherently at the SCM. The same holds true for the SCM-AP backward link. When $r > 1$, the scheme is not capacity-optimal because the SCM is intrinsically single-layer so that only one out of the r potential data streams, which could be established between the AP and the sensor, is exploited. However, it corresponds to the optimal single-layer beamforming scheme in the SNR maximization sense also providing the maximum diversity gain [34].

It is interesting to analyse the SNR in free-space condition assuming the AP and the SCM are in paraxial configuration at distance d. In this case, the SNR in (10) becomes

$$\mathsf{SNR} = \frac{P_{\mathrm{T}}\, g^2\, N^2\, M^2\, G_{\mathrm{AP}}^2\, G_{\mathrm{SCM}}^2\, \lambda^4}{\sigma^2\, (4\pi\, d)^4} \tag{11}$$

where G_{AP} and G_{SCM} are the gain of the elements of the AP's antenna and the SCM's cell, respectively. The last equation shows that, due to the backscattering nature of the communication, the path loss increases with the distance to the power of four, as expected in BackCom systems [20], [21], [22], [23]. On the other hand, such large path loss can be easily compensated by increasing the number of antenna elements N and M at the AP and sensor, respectively, as it will be investigated in Section VII.

Now, in order to establish the single-layer optimal communication between the sensor and the AP, the main problem to be solved is the fast detection of a new sensor and the fast and accurate estimation of the beamforming vector $\mathbf{v}_1$, especially in a multi-sensor MIMO scenario. In the next section, a fast and blind (i.e., without CSI estimation) scheme for joint eigenvectors estimation and multi-sensor communication is presented.

IV. Grant-Free Random Access Using MIMO SCMs

Consider a scenario in which a large number of asynchronous sensors deployed in the environment generate packets randomly. We consider the worst-case situation where each packet is generated by a distinct sensor located at

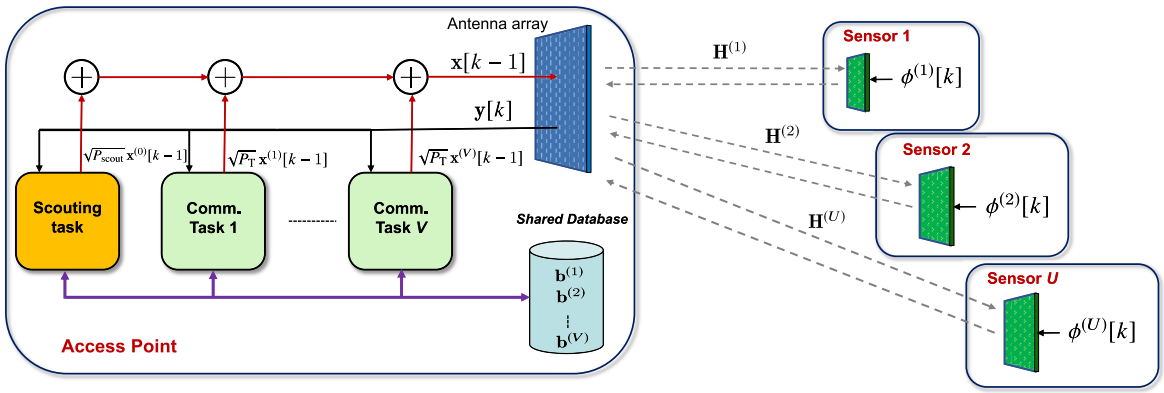

Fig. 2. Scheme of the proposed grant-free MIMO access based on SCMs.

a different location so that the reception of each packet requires the fast detection of the new sensor and the fast estimation of the beamforming vector at the AP without any a priori information. For this reason, in what follows we will interchange freely the terms packets and sensors. Note that in such a scenario, all the approaches relying on statistical/long-term CSI and/or sensors activity pattern estimation are highly inefficient or not applicable (e.g., [35]).

Suppose that, at the generic time interval, there are U asynchronous active (i.e., transmitting) sensors. Denote with $\mathbf{H}^{(1)}, \mathbf{H}^{(2)}, \ldots, \mathbf{H}^{(U)} \in \mathbb{C}^{M\times N}$ the channel matrices related to the U links between the AP and the active sensors. For further convenience, we define the corresponding modified round-trip channels $\mathbf{A}^{(u)} = g\,(\mathbf{H}^{(u)})^{\dagger}\mathbf{H}^{(u)} \in \mathbb{C}^{N\times N}$, for $u = 1, 2, \ldots, U$. In addition, we denote with $\mathbf{v}_i^{(u)}$ and $\lambda_i^{(u)}$, respectively, the i-th eigenvector and eigenvalue of $\mathbf{A}^{(u)}$, with $i = 1, 2, \ldots, r^{(u)}$, where $r^{(u)} = rank(\mathbf{A}^{(u)})$.

The main idea of the proposed grant-free MIMO access scheme is sketched in Fig. 2 and described in the following. The AP has several tasks running in parallel. In particular, one task, namely the *Scouting Task*, is always active and its purpose is to discover any newly transmitted[3] packet from a new active sensor and estimate the corresponding, possibly optimal, beamforming vector at the AP. Once a new packet is detected, the estimated beamforming vector, denoted as $\mathbf{b}^{(v)}$, is appended to a *Shared Database* that contains all the estimated beamforming vectors, indexed by v, related to the packets being decoded at that moment. In addition, a dedicated task, denoted as *Communication Task*, is initiated, and associated with the new packet. This task is responsible for decoding the packet until its completion. When the packet is over, i.e., the sensor stops backscattering, the associated Communication Task is terminated, and the corresponding beamforming vector is removed from the Shared Database. As it will be explained later, if $r^{(u)} > 1$, then the same packet transmitted by the u-th sensor might be decoded using different orthogonal beamforming vectors, each of them associated with a different eigenvalue of $\mathbf{A}^{(u)}$. As a consequence, the size of the Shared Database, and then the number V of instantiated Communication Tasks, might be in general equal or larger than the number U of currently active sensors, that is, $V \geq U$. In the following, let $u = f(v)$ represent the function that associates the packet currently being decoded by the v-th Communication Task with the index u of the corresponding sensor that generated it.

According to the scheme in Fig. 2, the Scouting Task and the V Communication Tasks generate, respectively, the beamforming vectors $\sqrt{P_{\text{scout}}}\,\mathbf{x}^{(0)}[k-1]$ and $\sqrt{P^{(v)}}\,\mathbf{x}^{(v)}[k-1] = \sqrt{P^{(v)}}\,\mathbf{b}^{(v)}$, $v = 1, 2, \ldots V$, which are summed up to form the actual transmitted vector $\mathbf{x}[k-1]$ at time $k-1$, that is,

$$\mathbf{x}[k-1] = \sum_{u=0}^{V} \sqrt{P^{(v)}}\,\mathbf{x}^{(v)}[k-1] \tag{12}$$

where $P^{(0)} = P_{\text{scout}}$ and $\mathbf{x}^{(0)}[k-1]$ are, respectively, the transmitted power and the current beamforming vector used by the Scouting Task. Without loss of generality, we assume that all the Communication Tasks transmit with the same power P_{T}, so $P^{(v)} = P_{\text{T}}$, $v = 1, 2, \ldots V$, even though power control schemes can be easily implemented to minimize the overall transmitted power. The signal received by the SCM of the u-th sensor during the k-th transmission interval is

$$\begin{aligned}\mathbf{z}^{(u)}[k] &= \mathbf{H}^{(u)}\,\mathbf{x}[k-1] + \boldsymbol{\eta}^{(u)}[k] \\ &= \mathbf{H}^{(u)} \sum_{l=0}^{V} \sqrt{P^{(l)}}\,\mathbf{x}^{(l)}[k-1] + \boldsymbol{\eta}^{(u)}[k]\end{aligned} \tag{13}$$

where $\boldsymbol{\eta}^{(u)}[k] \sim \mathcal{CN}(\mathbf{0}, \sigma_\eta^2\,\mathbf{I}_M)$ is the noise experienced by the SCM of the u-th sensor. In (13), the channel matrix $\mathbf{H}^{(0)}$ characterizes the communication link between the AP and a potential new sensor during the scouting process. More in general, $u \in \mathcal{U}$, where $\mathcal{U}$ is defined as the set $\{0, 1, 2, \ldots, U\}$, if a new sensor is detected; otherwise, $\mathcal{U} = \{1, 2, \ldots, U\}$. According to (2), the signal backscattered by the u-th sensor is $\mathbf{r}^{(u)}[k] = g\,e^{\jmath\phi^{(u)}[k]}(\mathbf{z}^{(u)}[k])^*$, then the signal received by the AP at the k-th time interval is given by the contributions from all sensors and can be written as

[3]For the sake of simplicity we say improperly that the sensor starts transmitting, whereas more precisely it starts backscattering the signal sent by the AP.

$$\begin{aligned}\mathbf{y}[k] &= \sum_{u\in\mathcal{U}} \left(\mathbf{H}^{(u)}\right)^T \mathbf{r}^{(u)}[k] + \mathbf{w}[k] \\ &= \sum_{u\in\mathcal{U}} e^{\jmath\phi^{(u)}[k]} \left(\mathbf{H}^{(u)}\right)^T \left(\mathbf{H}^{(u)}\right)^* \sum_{l=0}^{V} g\sqrt{P^{(l)}} \left(\mathbf{x}^{(l)}[k-1]\right)^* \\ &\quad + \mathbf{n}[k] \\ &= \sum_{u\in\mathcal{U}} e^{\jmath\phi^{(u)}[k]} \left(\mathbf{A}^{(u)}\right)^* \sum_{l=0}^{V} \sqrt{P^{(l)}} \left(\mathbf{x}^{(l)}[k-1]\right)^* + \mathbf{n}[k]\end{aligned} \tag{14}$$

where $\mathbf{A}^{(0)} = g\,(\mathbf{H}^{(0)})^\dagger \mathbf{H}^{(0)}$, $\mathbf{n}[k] = \mathbf{w}[k] + \sum_{u\in\mathcal{U}} (\mathbf{H}^{(u)})^T (\boldsymbol{\eta}^{(u)}[k])^*$ and $\{\phi^{(u)}[k]\}$ is the phase carrying the current data transmitted by the u-th active sensor. All the tasks have access to the received vector $\mathbf{y}[k]$.

The Shared Database (see Fig. 2), containing all the estimated beamforming vectors $\mathbf{B} = \{\mathbf{b}^{(1)}, \mathbf{b}^{(2)}, \cdots, \mathbf{b}^{(V)}\}$ associated with the packets currently being decoded, serves a dual purpose: *i)* the v-th beamforming vector $\mathbf{b}^{(v)}$ is used by the v-th Communication Task to address the sensor with index $u = f(v)$ until the end of the corresponding packet; *ii)* the set of beamforming vectors in $\mathbf{B}$ is used by the Scouting Task to perform the estimation of the beamforming vector of a possibly newly transmitting sensor in a subspace orthogonal to that spanned by the vectors in $\mathbf{B}$ (i.e., in the null space of $\mathbf{B}$). The latter ensures that the vectors in $\mathbf{B}$ are orthogonal and hence all the tasks (Scouting and Communication) address orthogonal subspaces. As a final remark, we note that the outlined analytical framework also accounts for potential misalignments of the beam reflected by sensors relative to the incident beam, due to the noise contribution in (13) that undergoes the conjugation operation fundamental to retrodirectivity. Likewise, the analysis incorporates the potential non-idealities in the beamforming vectors estimated by the AP, which are influenced by *i)* the presence of noise as well as by *ii)* sensor nodes oriented in non-orthogonal directions. The former affects the signal used by the AP for beamforming vectors' estimation, given by (14), while the latter ensures the beams are orthogonal to each other to avoid mutual interference, meaning that they may not be directed exactly toward the respective receivers. Remarkably, all these phenomena are accounted for in the numerical results of Section VI, where the outcomes of simulations will be presented.

A. Scouting Task

The pseudo-code of the algorithm executed by the Scouting Task is reported in Algorithm 1. At the startup time $k = 0$, $\mathbf{x}^{(0)}[0]$ is initialized with a unitary norm random vector (step 0 of the pseudo-code). At the $(k-1)$-th iteration, with $k > 1$, the Scouting Task (see Algorithm 1) sends the current estimated beamforming vector, $\mathbf{x}^{(0)}[k-1]$ (step 3), and receives back the response at time k from the new sensor (if any) according to (14) (step 4). Before further processing, the received vector $\mathbf{y}[k]$ is made orthogonal to $\mathbf{B}$, that is,

$$\mathring{\mathbf{y}}[k] = \left(\mathbf{I} - \mathbf{B}\,\mathbf{B}^\dagger\right)\mathbf{y}[k] \tag{15}$$

in order to force the searching in the null space of $\mathbf{B}$ and hence not interfere with the currently active Communication Tasks (step 5). Then, a normalized and conjugated version of $\mathring{\mathbf{y}}[k]$ is computed (step 6) and used as the updated beamforming vector $\mathbf{x}^{(0)}[k]$ in the subsequent iteration.

Algorithm 1: Algorithm of the Scouting Task

0: *Initialization*: generate a guess unitary norm beamforming vector $\mathbf{x}^{(0)}[0]$; $V = 0$;
1: **for** $k = 1, \ldots, \infty$ **do**
2: If the Shared Database has been updated, then generate a random unitary norm vector $\mathbf{x}^{(0)}[k-1]$ orthogonal to $\mathbf{B}$ //
3: transmit: $\sqrt{P_{\text{scout}}}\,\mathbf{x}^{(0)}[k-1]$ //
4: receive: $\mathbf{y}[k]$ //
5: $\mathring{\mathbf{y}}[k] = \text{orthogonalize}(\mathbf{y}[k], \mathbf{B})$ //
6: $\mathbf{x}^{(0)}[k] = (\mathring{\mathbf{y}}[k])^*/\|\mathring{\mathbf{y}}[k]\|$ `// beamforming vector update`
7: $\gamma[k] = \|\mathring{\mathbf{y}}[k]\|^2/\sigma^2$ `// SNR computation`
8: If $\gamma[k] > \gamma_{\text{dec}}$ and $\gamma[k]/\gamma[k-1] < \gamma_\Delta$, then a new packet has been detected, $V = V + 1$, a new dedicated Communication Task is allocated using $\mathbf{x}^{(0)}[k]$ as beamforming vector, and $\mathbf{b}^{(V)} = \mathbf{x}^{(0)}[k]$ is added to the Shared Database.
end

Finally, let k^* represent the time instant a new sensor starts the transmission of a packet. The new packet is detected when the SNR $\gamma[k] = \|\mathring{\mathbf{y}}[k]\|^2/\sigma^2$, with $k > k^*$, satisfies $\gamma[k] > \gamma_{\text{dec}}$ and $\gamma[k]/\gamma[k-1] < \gamma_\Delta$ (steps 7 and 8). The first inequality checks that a certain level of energy has been received compared to the noise level, whereas the second one guarantees that (16) is close to the convergence, with the thresholds γ_{dec} and γ_Δ to be properly tuned.

The processing operated by Algorithm 1 is the modification of the well-known *Power Method* [36] that, in the absence of noise, interference, and the orthogonalization in (15), allows the estimation of the top-eigenvector of the square matrix $\mathbf{A} = \sum_{u\in\mathcal{U}} \mathbf{A}^{(u)}$. Here, differently from the classical Power Method, due to (15), the matrix seen by the iterative method is $\mathring{\mathbf{A}} = (\mathbf{I} - \mathbf{B}\,\mathbf{B}^\dagger)\mathbf{A}$, which determines the subspace under exploration by the Scouting Task, whose eigenvectors and eigenvalues are denoted by $\{\mathring{\lambda}_1, \mathring{\lambda}_2, \ldots, \mathring{\lambda}_{\mathring{r}}\}$ and $\{\mathring{\mathbf{v}}_1, \mathring{\mathbf{v}}_2, \ldots, \mathring{\mathbf{v}}_{\mathring{r}}\}$, respectively, where $\mathring{r} = rank\left(\mathring{\mathbf{A}}\right)$. Furthermore, whenever a modification is made to $\mathbf{B}$ (such as adding or removing elements), $\mathbf{x}^{(0)}[k]$ is reinitialized by generating a random vector that is subsequently made orthogonal to the vectors in $\mathbf{B}$, according to (15), while ensuring it remains unitary. In particular, the beamforming vector is updated according to (step 6)

$$\mathbf{x}^{(0)}[k] = \frac{\mathring{\mathbf{y}}^*[k]}{\|\mathring{\mathbf{y}}[k]\|} \tag{16}$$

until a change on $\mathbf{B}$ occurs or a new packet is detected. In the absence of noise and interference, after a few iterations, the Power Method ensures that the direction of $\mathbf{x}^{(0)}[k]$ converges to that of the dominant eigenvector $\mathring{\mathbf{v}}_1$ of $\mathring{\mathbf{A}}$ [36].

Obviously, the new sensor can be detected only if $\mathring{\mathbf{A}}$ and $\mathbf{A}^{(0)}$ share a not null subspace. It has to be remarked that, in general, it is not guaranteed that $\mathring{\mathbf{v}}_1$ is referred to the channel between the AP and the new sensor. In fact, when the sensor and AP are in radiating near-field conditions, or in far-field in the presence of multipath, the channel might have a rank larger than one and the same sensor can be reached addressing different orthogonal subspaces [37]. In such cases,

Algorithm 2: Algorithm of the v-th Communication Task

0: *Initialization*: *active* $= 1$, $k = k^{(v)}$ // $k^{(v)}$ time instant of packet detection
1: **while** *active=1* **do**
2: transmit: $\sqrt{P^{(v)}}\,\mathbf{x}^{(v)}[k-1] = \sqrt{P^{(v)}}\,\mathbf{b}^{(v)}$ //
3: receive: $\mathbf{y}[k]$ //
4: $u^{(v)}[k] = \left(\mathbf{b}^{(v)}\right)^{\dagger}\mathbf{y}^{*}[k]$ // decision variable
5: $\widehat{\phi}[k] = \text{demodulation}\left(-\arg\left\{u^{(v)}[k]\right\}\right)$ // data demodulation
6: $\gamma[k] = \left|u^{(v)}[k]\right|^2/\sigma^2$ // SNR computation
7: If $\gamma[k] < \gamma_{\text{drop}}$, then beamforming vector $\mathbf{b}^{(v)}$ is removed from the Shared Database and this task is de-instantiated ($active = 0$, $V = V - 1$) //
$k = k + 1$;
end

the Scouting Task is likely to converge to a subspace related to a sensor already under decoding but not yet included in $\mathbf{B}$, and hence a second Communication Task will be associated with that sensor. Duplicated packet decoding is not an issue as it can be easily solved by higher protocol layers. On the contrary, such a phenomenon might be beneficial as it creates a sort of eigenvector diversity. If the packet generation of the new sensor is not simultaneous (at symbol time T level) to the generation of an already serving sensor, it is likely that all the significative secondary eigenvectors of $\mathring{\mathbf{A}}$ have been already explored when the new sensor starts its transmission, and $\mathbf{v}_1^{(0)}$ is effectively associated with the new sensor, as we will assume in the rest of the paper.

B. Communication Task

Once a new packet has been detected by the Scouting Task, a new Communication Task is activated whose algorithm is reported in Algorithm 2. Denote with $k^{(v)}$ the time instant the packet is detected by the Scouting Task and the Communication Tasks starts, being v the index associated to the new packet generated by the u-th sensor, with $u = f(v)$, and with $\mathbf{b}^{(v)} = \mathbf{x}^{(0)}[k^{(v)}]$ the corresponding beamforming vector estimated through Algorithm 1 and stored in the Shared Database by the Scouting Task. The Communication Task, for $k \geq k^{(v)}$ until the end of the packet, executes Algorithm 2 that, at each iteration, always transmits the same beamforming vector $\sqrt{P^{(v)}}\,\mathbf{x}^{(v)}[k-1]$, with $\mathbf{x}^{(v)}[k-1] = \mathbf{b}^{(v)}$ (step 2). Subsequently, according to (8) and (14), the decision variable is formed as (step 4)

$$\begin{aligned} u^{(v)}[k] &= \left(\mathbf{b}^{(v)}\right)^{\dagger}\mathbf{y}^{*}[k] \\ &= \sum_{i\in\mathcal{U}} e^{-\jmath\phi^{(i)}[k]}\left(\mathbf{b}^{(v)}\right)^{\dagger}\mathbf{A}^{(u)}\sum_{l=0}^{V}\sqrt{P^{(l)}}\,\mathbf{x}^{(l)}[k-1] \\ &\quad + \left(\mathbf{b}^{(v)}\right)^{\dagger}\mathbf{n}^{*}[k] \\ &= e^{-\jmath\phi^{(u)}[k]}\sum_{l=0}^{V}\sqrt{P^{(l)}}\left(\mathbf{b}^{(v)}\right)^{\dagger}\mathbf{A}^{(u)}\,\mathbf{x}^{(l)}[k-1] \\ &\quad + \sum_{i\in\mathcal{U},\, i\neq u}^{U} e^{-\jmath\phi^{(i)}[k]}\sum_{l=0}^{V}\sqrt{P^{(l)}}\left(\mathbf{b}^{(v)}\right)^{\dagger}\mathbf{A}^{(u)}\,\mathbf{x}^{(l)}[k-1] \\ &\quad + \left(\mathbf{b}^{(u)}\right)^{\dagger}\mathbf{n}^{*}[k] \end{aligned} \tag{17}$$

where $u = f(v)$. A decision on the transmitted phase $\phi^{(u)}[k]$ from the sensor with index $u = f(v)$ is made (step 5) based on the argument of $u^{(v)}[k]$ in (17) according to the mapping scheme considered, as explained in Section III. The first term in (17) represents the useful contribution. Equation (17) reveals that, in general, the decision variable is affected by the presence of interference from other sensors (second term), caused by potential not orthogonality of the sensors' channels, and thermal noise (third term). Finally, when $\gamma[k] = |u^{(v)}[k]|^2/\sigma^2 < \gamma_{\text{drop}}$, the end of the packet has been likely reached, and the task is deactivated (steps 6 and 7).

C. Orthogonal Channels (Favorable Propagation)

Equation (17) shows that, depending on channel characteristics, the decision variable might be deteriorated by the presence of inter-sensor interference.

Consider the scenario in which the subspaces spanned by $\mathbf{H}^{(u)}$ are orthogonal to each other, and so those by $\mathbf{A}^{(u)}$, for $u \in \mathcal{U}$. This implies that $(\mathbf{v}_n^{(v)})^{\dagger}\mathbf{A}^{(u)}\,\mathbf{v}_m^{(l)}$ is different from zero only when $v = l$ and $m = n$. This assumption can be in general approached when sensors are located in different positions and a large number of antennas is used at the AP [38]. This condition is typically referred to as *favorable propagation* in massive MIMO literature. For instance, in [39] it has been shown that the favorable propagation condition can be approached even in correlated Rayleigh and geometry-based multi-sensor MIMO channels when N grows.

Under favorable propagation and assuming an accurate estimation of the eigenvectors has been achieved by the Scouting Task, such that $\mathbf{b}^{(v)} \simeq \mathbf{v}_i^{(u)}$, with $u = f(v)$, for some $i \in \{1, 2, \ldots, r^{(u)}\}$, the inter-sensor interference terms become negligible and (17) simplifies to

$$\begin{aligned} \mathbf{u}^{(v)}[k] &\simeq \sqrt{P_{\text{T}}}\,e^{-\jmath\phi^{(u)}[k]}\left(\mathbf{b}^{(v)}\right)^{\dagger}\mathbf{A}^{(u)}\,\mathbf{b}^{(v)} \\ &\quad + \left(\mathbf{b}^{(v)}\right)^{\dagger}\mathbf{n}^{*}[k] \\ &\simeq \sqrt{P_{\text{T}}}\lambda_i^{(u)}e^{-\jmath\phi^{(u)}[k]} + n_i[k] \end{aligned} \tag{18}$$

like in the single-sensor case in (9) because $\mathbf{b}^{(v)}$ is an eigenvector of the round-trip time channel matrix $\mathbf{A}^{(u)}$. In addition, $\mathring{\mathbf{A}} = \mathbf{A}^{(0)}$ and $\mathring{\mathbf{v}}_1 = \mathbf{v}_1^{(0)}$, that is, the top-eigenvector of $\mathbf{A}^{(0)}$.

V. Convergence Analysis of the Scouting Task

In this section, we investigate the converge properties of the proposed iterative approach, inspired by the Power Method, applied during the Scouting Task to estimate the top eigenvector of the channel matrix. Note that Power methods have already been investigated for estimating the top eigenvectors of MIMO channels in time-division communication systems [40]. However, in these systems, both the AP and the sensor must possess substantial signal processing capabilities to implement signal decoding and QR decomposition, whereas, in our backscatter communication system, no signal processing is required at the sensor. Furthermore, to the best of the authors' knowledge, the noise introduced in the system and the presence of data have never been considered in the Power

Method convergence analysis. In fact, the main issue is that at each iteration, new noise and data components enter the loop. Therefore, convergence towards the top eigenvector is not always guaranteed and the Scouting Task may instead converge towards the noise.

The convergence behavior of the Scouting Task, given that a new sensor has started its transmission, can be analysed assuming that no other sensor starts its transmission during the first symbols of the packet and/or has its channel subspace partially overlapped in the subspace spanned by $\mathring{\mathbf{A}}$. In the presence of noise, (16) reads

$$\mathbf{x}^{(0)}[k] = \frac{\mathring{\mathbf{y}}^*[k]}{\|\mathring{\mathbf{y}}[k]\|} = \frac{\sqrt{P_{\text{scout}}}\,\mathring{\mathbf{A}}\, e^{-\jmath\phi[k]}\mathbf{x}^{(0)}[k-1] + \mathbf{n}[k]}{\left\|\sqrt{P_{\text{scout}}}\,\mathring{\mathbf{A}}\, e^{-\jmath\phi[k]}\mathbf{x}^{(0)}[k-1] + \mathbf{n}[k]\right\|} \tag{19}$$

where

$$\mathring{\mathbf{y}}^*[k] = \sum_{j=1}^{N} \mathring{\mathbf{v}}_j \left(\sqrt{P_{\text{scout}}}\,\mathring{\lambda}_j x_j[k-1] e^{-\jmath\phi[k]} + n_j[k]\right) \tag{20}$$

and $x_j[k]$, $n_j[k] \sim \mathcal{CN}(0,\sigma^2)$ represent, respectively, the projections of $\mathbf{x}^{(0)}[k]$, $\mathbf{n}[k]$ onto $\mathring{\mathbf{v}}_j$. Note that the term carrying the information (i.e., the phase $\phi[k]$) also includes the noise from the previous iterations, which is contained in $x_j[k-1]$. In fact, here both the signal and the noise components are reflected by the SCM and possibly amplified if active, i.e., $g > 1$. Moreover, $|x_j[k-1]|^2/\|\mathbf{x}^{(0)}[k-1]\|^2 = |x_j[k-1]|^2$, being $\|\mathbf{x}^{(0)}[k]\|^2 = 1$, represents the fraction of the total transmitted power (useful plus noise) associated to direction $\mathring{\mathbf{v}}_j$ at the discrete time $k-1$. Then, at the end of the k-th time interval, the received SNR along the direction $\mathring{\mathbf{v}}_j$ is given by

$$\mathsf{SNR}_j[k] = \frac{P_{\text{scout}}\,\mathring{\lambda}_j^2\,|x_j[k-1]|^2}{\sigma^2}. \tag{21}$$

The goal is to determine an iterative expression for $\mathsf{SNR}_j[k]$, which drives the signal demodulation performance in the Communication Task and evaluate the convergence condition of the Scouting Task we proposed. Considering (20), the fraction of the total power that is associated with direction $\mathring{\mathbf{v}}_j$ at the beginning of time interval k can be written as

$$|x_j[k]|^2 = \frac{P_{\text{scout}}\,\mathring{\lambda}_j^2\,|x_j[k-1]|^2 + \sigma^2}{\sum_{i=1}^{N}\left(P_{\text{scout}}\,\mathring{\lambda}_i^2\,|x_i[k-1]|^2 + \sigma^2\right)}. \tag{22}$$

By inverting (21) and plugging $|x_j[k]|^2$ at both the left-hand and right-hand sides of (22), we obtain the following iterative formula for $\mathsf{SNR}_j[k]$

$$\begin{aligned}\mathsf{SNR}_j[k] &= \frac{P_{\text{scout}}\,\mathring{\lambda}_j^2\big(\mathsf{SNR}_j[k-1]+1\big)}{\sigma^2\left[\sum_{i=1}^{N}(\mathsf{SNR}_i[k-1]+1)\right]} \\ &= \mathsf{SNR}_j^{(\max)}\frac{\mathsf{SNR}_j[k-1]+1}{N+\sum_{i=1}^{\mathring{r}}\mathsf{SNR}_i[k-1]}\end{aligned} \tag{23}$$

for $j = 1,2,\ldots,\mathring{r}$, and $k \geq k^*$, being k^* the time instant the new sensor started the transmission, where $\mathsf{SNR}_j[k^*] = \mathsf{SNR}_j^{(\max)}|x_j[k^*]|^2$, and

$$\mathsf{SNR}_j^{(\max)} = \frac{P_{\text{scout}}\,\mathring{\lambda}_j^2}{\sigma^2}. \tag{24}$$

The quantity $\mathsf{SNR}_j^{(\max)}$ represents the maximum SNR along the direction $\mathring{\mathbf{v}}_j$, i.e., the SNR one would obtain if all the power was concentrated to direction $\mathring{\mathbf{v}}_j$. Note that if $\mathbf{x}[k^*]$ is initialized randomly, then $|x_j[k^*]|^2 \simeq 1/N$ so that $\mathsf{SNR}_j[k^*] \simeq \mathsf{SNR}_j^{(\max)}/N$.

In the particular but common case where channel $\mathring{\mathbf{A}}$ has rank 1, the SNR at the k-th time instant along direction $\mathring{\mathbf{v}}_1$ in (23) simplifies into

$$\mathsf{SNR}_1[k] = \mathsf{SNR}_1^{(\max)}\frac{\mathsf{SNR}_1[k-1]+1}{N+\mathsf{SNR}_1[k-1]} \tag{25}$$

for $k \geq k^*$, which allows an easy evaluation of the convergence value. At the convergence it must be $\mathsf{SNR}_1[k] \simeq \mathsf{SNR}_1[k-1]$ then, by dropping the time index, (25) becomes the quadratic equation

$$\mathsf{SNR}_1 = \mathsf{SNR}_1^{(\max)}\frac{\mathsf{SNR}_1+1}{N+\mathsf{SNR}_1} \tag{26}$$

whose positive solution is

$$\mathsf{SNR}_1 = \frac{1}{2}\left(N - \mathsf{SNR}_1^{(\max)} + \left|\mathsf{SNR}_1^{(\max)} - N\right|\sqrt{1+\frac{\mathsf{SNR}_1^{(\max)}}{\left(\mathsf{SNR}_1^{(\max)}-N\right)^2}}\right). \tag{27}$$

Denote with $\mathsf{SNR}_1^{(\text{boot})} = \mathsf{SNR}_1^{(\max)}/N$ the *bootstrap* SNR. Upon inspection of (27) it becomes evident that if $\mathsf{SNR}_1^{(\text{boot})} \gg 1$, then at convergence it is $\mathsf{SNR}_1 \simeq \mathsf{SNR}_1^{(\max)} - N \simeq \mathsf{SNR}_1^{(\max)} \gg 1$, which takes the role of asymptotic SNR corresponding to the optimum beamforming vector for a channel with rank 1. When the bootstrap SNR is much less than one, we still have convergence but at $\mathsf{SNR}_1 \ll 1$ so that the link cannot be established. It is worth noticing that the convergence value does not depend on the initial random guess, but only on the bootstrap SNR. According to (11), the link budget can be ameliorated by increasing M and/or N indifferently as both play quadratically. On the contrary, the bootstrap SNR increases quadratically with M but only linearly with N, therefore it is better to increase M than N, when possible. The convergence analysis for $\mathring{r} > 1$ involves the evaluation of an $\mathring{r}+1$ polynomial equation that becomes not feasible analytically for large r. Despite that, numerical investigations reported in the next section put in evidence that the previous condition to reach the asymptotic SNR holds even when $\mathring{r} > 1$ so that, upon convergence, $|x_1[k]| \gg |x_j[k]|$ for $j > 1$.

When the Scouting Task detects the new sensor, suppose it at the time interval $\tilde{k}$, $\mathbf{x}^{(0)}[\tilde{k}]$ is used as an estimate of the top-eigenvector $\mathring{\mathbf{v}}_1$ in the Communication Task that will be associated to the sensor. Such an estimate is characterized by $\mathsf{SNR}_1[\tilde{k}]$ that can be computed through the iterative

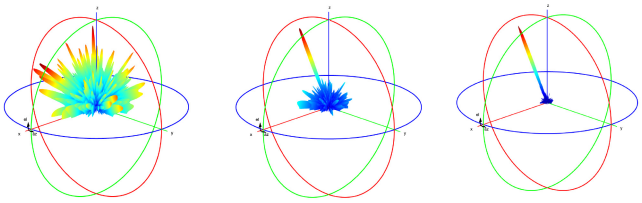

(a) (b) (c)

Fig. 3. Evolution of the beam's shape at time $k = 1$ (a), $k = 2$ (b), and $k = 3$ (c).

formula (23). The decision variable $u[k]$ at the k-th symbol is proportional to the product

$$u[k] \propto \mathbf{x}^{\dagger}\left[\tilde{k}\right]\mathbf{y}^{*}[k] = \sqrt{P_{\mathrm{T}}}e^{-\jmath\phi[k]}\sum_{j=1}^{\mathring{r}}\mathring{\lambda}_j\left|x_j\left[\tilde{k}\right]\right|^2 + \mathbf{x}^{\dagger}\left[\tilde{k}\right]\mathbf{n}[k] \tag{28}$$

in which the first term is the useful one, as it contains the phase $\phi[k]$ that carries the information, and the second term represents the noise. Since $\|\mathbf{x}[\tilde{k}]\|^2 = 1$, the SNR at the input of the detector is

$$\mathsf{SNR}^{(\mathrm{dec})} = \frac{P_{\mathrm{T}}\left(\sum_{j=1}^{\mathring{r}}\mathring{\lambda}_j\left|x_j\left[\tilde{k}\right]\right|^2\right)^2}{\sigma^2}. \tag{29}$$

Therefore, we can rewrite (29) as a function of $\mathsf{SNR}_j[k]$ as

$$\mathsf{SNR}^{(\mathrm{dec})} = \frac{P_{\mathrm{T}}}{P_{\mathrm{scout}}}\left(\sum_{j=1}^{\mathring{r}}\frac{\mathsf{SNR}_j\left[\tilde{k}\right]}{\sqrt{\mathsf{SNR}_j^{(\max)}}}\right)^2 \simeq \frac{P_{\mathrm{T}}}{P_{\mathrm{scout}}}\mathsf{SNR}_1^{(\max)} = \frac{P_{\mathrm{T}}\,\mathring{\lambda}_1^2}{\sigma^2}. \tag{30}$$

In the case of favorable propagation, it is

$$\mathsf{SNR}^{(\mathrm{dec})} \simeq \frac{P_{\mathrm{T}}\left(\lambda_1^{(0)}\right)^2}{\sigma^2} \tag{31}$$

which resembles (10) of the single-sensor scenario.

Notice that the precoding vector $\mathbf{x}[k]$, transmitted at the instant k, determines the shape of the beam according to classic antenna array theory. At the beginning of the Scouting Task, i.e., at $k = 0$, the beam takes a random shape because the sensor's position is unknown, and consequently, $\mathbf{x}[0]$ is chosen randomly. During the iterative algorithm, the shape of the transmitted beam evolves from a random shape to the top right eigenvector of the channel. In free-space conditions, this corresponds to beam steering toward the intended user, whereas in a more complex propagation setting (e.g., with multipath), it might take a more articulated shape. In Fig. 3, a graphical example of the evolution of the beam's shape is illustrated in free-space condition. Note that the beam converges very fast to the final shape.

VI. Numerical Results

In this section, we report some simulation results with the purpose of investigating the performance of the proposed scheme. The values of the system parameters adopted for the analysis and the simulations are reported in Table I (some will be defined later), if not otherwise specified. The scenario considered, shown in Fig. 4, is composed of an AP, equipped with a uniform planar array (UPA) deployed along the xy-plane, located at (0, 0,0) [m], and sensors generating very short packets of total length $K = 144$ bits (18 bytes payload). In particular, packets are generated randomly with exponentially distributed inter-arrival time with mean μ, corresponding to a total offered traffic $G = T_{\mathrm{p}}/\mu$, where $T_{\mathrm{p}} = K\,T$ is the packet duration. Each packet corresponds to a sensor whose position is generated randomly with uniform distribution within the area centred in (0, 0, 10) [m] and size $20 \times 20\,[\mathrm{m}^2]$. The sensor's SCMs are supposed to lay on the xy-plane.

In Fig. 5(a), the time evolution of $\mathsf{SNR}_1[k]$ during the Scouting Task is shown for different bootstrap conditions in the case of rank-1 channel computed using (23), with $k^* = 1$. In the first 2 top curves, a random initial guess of the beamforming vector, corresponding to $\mathsf{SNR}_1[1] \simeq \mathsf{SNR}_1^{(\max)}/N$, was assumed, whereas the third curve is related to an even

TABLE I
Parameters Used in the Simulation

Parameter	Symbol	Value
Carrier frequency	f_{c}	100 GHz
AP antenna element gain	G_{AP}	0 dB (isotropic)
SCM cell gain	G_{SCM}	0 dB (isotropic)
SCM backscatter gain	g	20 dB
Bandwidth	W	10 MHz
Symbol time	T	100 ns
TX power	P_{T}	-5 dBm
Power boost scouting	$P_{\mathrm{scout}}/P_{\mathrm{T}}$	10 dB
SCM noise figure	F_{SCM}	3 dB
AP noise figure	F_{AP}	3 dB
AP antenna elements	N	30×30 ($4.5 \times 4.5\,\mathrm{cm}^2$ UPA)
SCM cells per sensor	M	20×20 ($3 \times 3\,\mathrm{cm}^2$ UPA)
Path loss exponent	β	2
Detection SNR threshold	γ_{dec}	30 dB
Delta SNR convergence	γ_{Δ}	5 dB
Drop SNR threshold	γ_{drop}	5 dB
Packet length	K	144 bits
Guard symbols	K_{g}	16 bits
Packet duration	$T_{\mathrm{p}} = K\,T$	14.4 μs

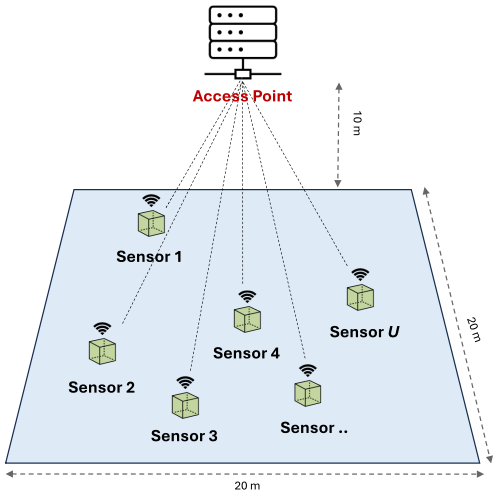

Fig. 4. Simulated scenario.

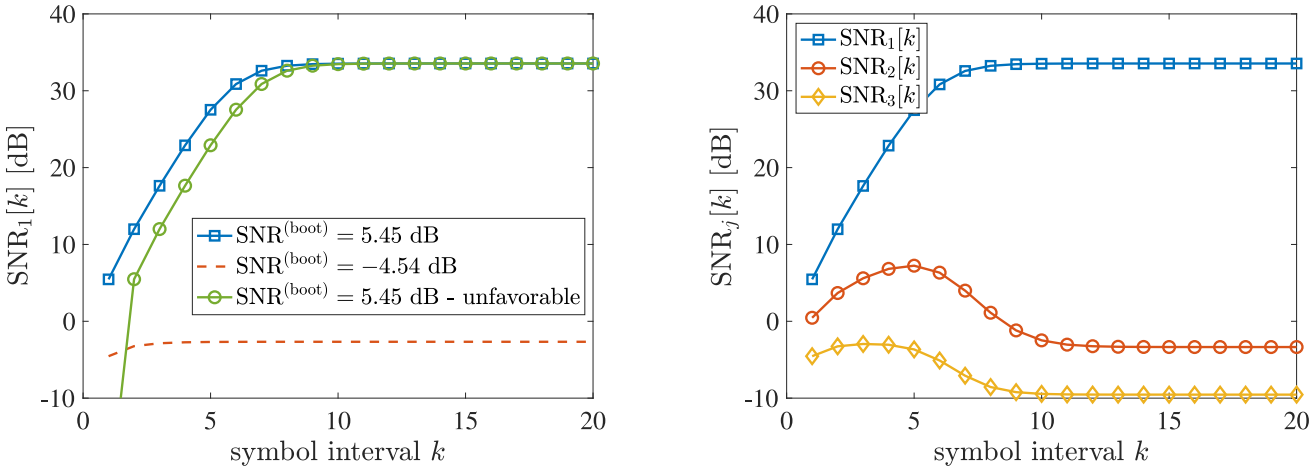

Fig. 5. Time evolution of the SNR during the Scouting Task for different bootstrap conditions in the case of rank-1 channel (a) - $\mathsf{SNR}_1[k]$, and rank-3 channel (b) - $\mathsf{SNR}_j[k]$).

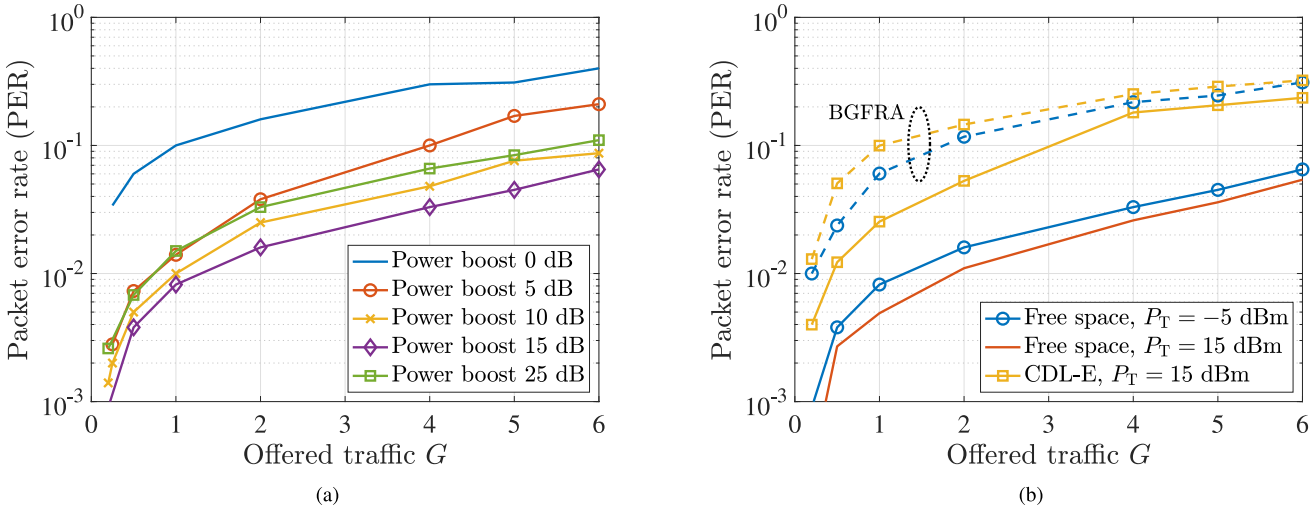

Fig. 6. (a): Packet error rate as a function of the offered traffic G. Effect of the Scouting Task power boost. $P_{\text{T}} = -5$ dBm. Free space condition. (b): Packet error rate as a function of the offered traffic G for different transmitted power levels and channel models. Power boost 15 dB.

more unfavorable situation where $\mathsf{SNR}_1[1] = \mathsf{SNR}_1^{(\max)}/N^2$. The blue and green curves have been evaluated with $\mathsf{SNR}_1^{(\max)} = 35$ dB and $\mathsf{SNR}_1^{(\max)} = 25$ dB, respectively, to which a bootstrap SNR of 5.45 dB and −4.54 dB corresponds. It can be noticed that when the bootstrap SNR is larger than one, the SNR converges after a few steps to $\mathsf{SNR}_1^{(\max)}$ and the packet can be detected, whereas it converges to a very low SNR when the bootstrap SNR is less than one, as predicted by (27). From Fig. 5(a), it can also be concluded that the impact of the initial beamforming vector on the SNR evolution is marginal, and it does not affect the final value.

The situation with a rank-3 channel (e.g., due to multipath) is analysed in Fig. 5(b), where the evolution of $\mathsf{SNR}_j[k]$, $j = 1, 2, 3$, is plotted for $\mathsf{SNR}_1^{(\max)} = 35$ dB, $\mathsf{SNR}_2^{(\max)} = 30$ dB, and $\mathsf{SNR}_3^{(\max)} = 25$ dB. As evident in the figure, the proposed iterative method ensures the convergence to the top eigenvector of the channel (blue curve), whereas the components associated with the top-second and top-third eigenvectors vanish. Comparing the blue curves in Fig. 5(a) and Fig. 5(b), it can also be observed that the convergence speed to the top-eigenvector is only slightly affected by the channel rank. In all cases, the convergence time is below 10 time intervals. This suggests that a guard time of $K_{\text{g}} = 16$ symbols set to zero, inserted at the beginning of each packet and followed by the payload of 32 bytes, gives sufficient time to the Scouting Task to converge and detect the packet.

Since the Scouting Task is the most critical one, it is of interest to investigate whether it benefits from an assignment of a power level P_{scout} higher than the power level P_{T} associated with the Communication Task. To this purpose, we define the power boost as $P_{\text{scout}}/P_{\text{T}}$. In Fig. 6(a), the packet error rate (PER), corresponding to $1 -$ {Probability of packet detection}, as a function of the offered traffic G is shown for different scouting power boost levels in free space. The PER has been computed through Monte Carlo simulations terminated when at least 100 erroneous packets were

counted. Observations reveal that the benefits of the power boost do not escalate indefinitely, indicating the presence of a discernible trade-off. Indeed, while increasing the power boost aids in detecting new packets by the Scouting Task, it may also increase interference for packets already undergoing decoding, particularly in unfavorable propagation conditions. Simulations demonstrate that a power boost of 15 dB yields the lowest PER across all scenarios, yet satisfactory performance is still achieved with a lower boost level of 10 dB. Obviously, under favorable propagation (massive MIMO) the inter-sensor interference is minimized, and the determination of the power boost is less critical.

The impact of the transmitted power and channel models can be observed in Fig. 6(b). In particular, free-space and the LOS CDL-E multipath 3GPP channel models [41] with a delay spread of 9 ns have been considered. With multipath, slightly higher power levels are in general necessary to satisfy the link budget. The increase of the transmitted power lowers slightly the PER indicating that the performance is mainly limited by the inter-sensor interference caused by the non-orthogonality of the channels in this scenario. The curves denoted with baseline GFRA (BGFRA) will be described in Section VII. Achieving favorable propagation, i.e., channel orthogonality, through a substantial increase of the antenna elements at the AP is one possible solution to mitigate or even eliminate the inter-sensor interference and hence significantly improve the performance. Another possible solution to mitigate the effect of the interference is to introduce a successive interference cancellation (SIC) algorithm, for instance a NOMA scheme, as it will be discussed in Section VII.

VII. Comparison With Baseline Solutions

In this section, our goal is to highlight the differences between our work and the existing literature on GFRA and metasurface-based BackCom schemes, while clarifying the strengths and weaknesses of our proposed SCM-based solution.

A. SCM-Based vs Baseline Massive MIMO GFRA

Some might argue that a potential drawback of the proposed scheme based on backscatter communication, in comparison to conventional GFRA schemes, is the increased path loss resulting from the two-way channel. This observation might lead to the conclusion that the proposed SCM-based scheme may not be suitable for operation in high-frequency bands, such as mmWaves or even THz. On the contrary, as it will be analysed in the following, this is a wrong conclusion.

A typical GFRA scheme employs single antenna sensors with a single RF chain and possibly a multi-antenna AP, i.e., an uplink SIMO configuration, even though it is often referred to as "massive MIMO", as already outlined in the Introduction. In this scenario, each sensor employs a preamble from a limited set of orthogonal sequences for detection and channel estimation purposes at the AP. As a consequence, for a given preamble length, the performance is bounded by the limited number of available preambles [10]. Moreover, in traditional GFRA systems, the benefit of path loss recovery, made possible in principle by the MIMO technology, cannot be practically achieved when dealing with sensing nodes. In fact, a MIMO solution is in general not feasible for two main reasons: *i)* if sensors are only transmitting, they do not have a chance to perform beamforming because of the lack of CSI; *ii)* even though sensors were equipped also with a receiver, the complexity required for estimating the CSI and performing beamforming, including the need for an antenna array with phase shifters and signaling overhead, might not be affordable, especially at high frequencies.

Therefore, in order to perform a fair comparison, we consider a SIMO BGFRA system which is supposed to have a complexity similar to that of the proposed SCM-based scheme. For simplicity, we consider free space propagation, and we compare the SCM-based and BGFRA schemes by fixing the size of the AP antenna array $A_{\mathrm{AP}} \simeq N\lambda^2/4$ and the sensor SCM size $A_{\mathrm{SCM}} \simeq M\lambda^2/4$, assuming antenna elements are spaced apart of $\lambda/2$. Under this condition, from (25) the maximum SNR can be expressed as a function of the antenna sizes, yielding

$$\begin{aligned}\mathsf{SNR}^{(\mathrm{SCM})} &= \frac{P_{\mathrm{T}}\, g^2\, N^2\, M^2\, G_{\mathrm{AP}}^2\, G_{\mathrm{SCM}}^2\, \lambda^4}{\sigma^2\,(4\pi d)^4} \\ &= \frac{P_{\mathrm{T}}\, g^2\, 16 A_{\mathrm{AP}}^2\, G_{\mathrm{AP}}^2\, 16 A_{\mathrm{SCM}}^2\, G_{\mathrm{SCM}}^2}{\lambda^4 \sigma^2\,(4\pi d)^4}. \end{aligned} \tag{32}$$

The last equation highlights that by maintaining a constant area for the antenna arrays, the SNR increases with the fourth power of the frequency (i.e., the inverse of λ), despite the greater propagation loss associated with higher frequencies.

For the BGFRA scheme, the maximum achievable SNR (perfect CSI estimate), assuming the gain of the sensor's transmitting antenna is equal to G_{SCM}, is

$$\begin{aligned}\mathsf{SNR}^{(\mathrm{BGFRA})} &= \frac{P_{\mathrm{T}}\, N\, G_{\mathrm{AP}}\, G_{\mathrm{SCM}}\, \lambda^2}{\sigma^2\,(4\pi d)^2} \\ &= \frac{4\, P_{\mathrm{T}}\, A_{\mathrm{AP}}\, G_{\mathrm{AP}}\, G_{\mathrm{SCM}}}{\sigma^2\,(4\pi d)^2} \end{aligned} \tag{33}$$

which is constant with the frequency. Comparing (32) and (33), it is $\mathsf{SNR}^{(\mathrm{SCM})} > \mathsf{SNR}^{(\mathrm{BGFRA})}$ when

$$f_{\mathrm{c}} > c\,\sqrt{4\pi d}\,\alpha^{-\frac{1}{4}} \tag{34}$$

where $\alpha = g^2\, 64\, A_{\mathrm{AP}}\, G_{\mathrm{AP}}\, A_{\mathrm{SCM}}^2\, G_{\mathrm{SCM}}$ and c is the speed of light. The previous inequality provides the condition on the carrier frequency under which our backscatter-based SCM scheme leads to a more favorable link budget than that of a BGFRA scheme.

In Fig. 7(a), the discriminating carrier frequency given in (34) is plotted for $\alpha = -70, -60, -50$ dB corresponding, respectively, to the values in Table I for $g = 0$, 10, 20 dB. Obviously, the same values can be obtained through different combinations of the factors determining α such as the antenna size. The area above each curve represents the frequency/distance combinations for which our scheme is more advantageous in terms of link budget. As it can be observed, despite its backscatter nature, the two-way path loss

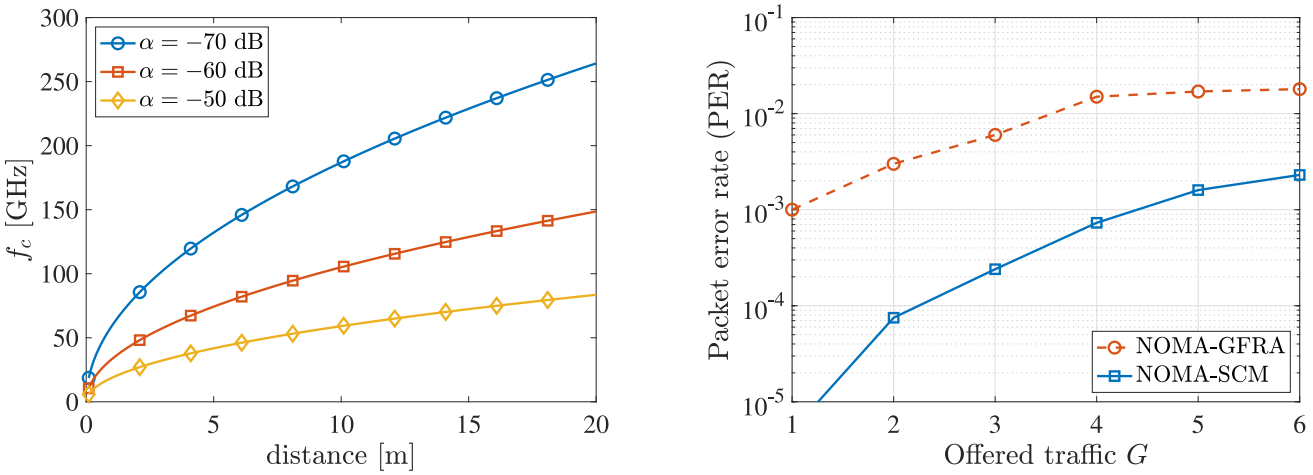

(a) (b)

Fig. 7. (a): Carrier frequency above that our SCM-based scheme provides a more favorable link budget with respect to a Ş BGFRA scheme using the parameters in Table I. Free-space condition. (b): Comparison between NOMA-SCM and NOMA-GFRA. $P_{\mathrm{T}} = -5\,\mathrm{dBm}$. Free-space condition.

is compensated and overcome by the two-way MIMO antenna gain making our scheme particularly appealing when working at high frequencies and/or small distances.

In terms of performance comparison, we consider as reference the analysis carried out in [10] for the BGFRA. Assuming a perfect CSI estimation, a preamble length equal to K_{g} (same overhead as our scheme) chosen randomly among all possible $K_{\mathrm{p}} = 2^{K_{\mathrm{g}}}$ preambles, a BPSK uncoded modulation, the packet error probability (PEP) can be computed as

$$P_e = 1 - P_{\mathrm{nc}}(K_{\mathrm{p}}) \prod_{k=K_{\mathrm{g}}+1}^{K} \left(1 - \frac{1}{2}\mathrm{erfc}\left(\sqrt{\mathrm{SINR}_k}\right)\right) \quad (35)$$

where $\mathrm{erfc}(\cdot)$ is the complementary error function, SINR_k is the signal-to-interference-noise ratio (SINR) of the k-th received symbol, and $P_{\mathrm{nc}}(K_{\mathrm{p}})$ represents the probability of no preamble collision given by [10]

$$P_{\mathrm{nc}}(K_{\mathrm{p}}) = \left(1 - \frac{1}{K_{\mathrm{p}}}\right)^{N_{\mathrm{i}}} \quad (36)$$

with N_{i} being the number of interfering packets. SINR_k and N_{i} have been obtained under the same simulation scenario whose parameters are listed in Table I. As it can be noticed in (35), the packet error probability is affected by both the probability of preamble collision and the probability of correct packet detection.

In Fig. 6(b), the PEP of the BGFRA scheme is compared with the PER of the SCM scheme under the same conditions. It can be observed that due to preamble collision and a less favorable link budget, as explained before, the BGFRA scheme provides a worse performance compared to the backscatter SCM-based scheme. Through a more detailed numerical investigation of the components of (35), we found out that the dominant performance degradation factor is given by preamble collisions rather than non-perfect channel orthogonality which is similar for both schemes since they work in the same scenario. Preamble collisions can be reduced by increasing the size of the preamble at the expense of a significant overhead when short packet transmission is considered. While the performance of BGFRA is compromised by pilot collisions, our approach is only limited by non-perfect orthogonality stemming from geometric configuration. In the case of quasi-perfect orthogonality, for instance by going massive with the number of antennas, the performance of our scheme would perform similarly to the single-sensor scenario whereas BGFRA schemes would be still limited by preamble collision.

B. NOMA-Based SCM and GFRA

As anticipated, the impact of the interference caused by non-perfect channel orthogonality can be mitigated by introducing a NOMA scheme as recently considered in state-of-the-art GFRA algorithms [12]. Specifically, this can be done by applying a SIC algorithm during the Communication Task which is in charge of decoding all the packets that are significantly colliding in the same channel subspace spanned by the precoding vector associated with that Communication Task. To this end, the Communication Task is kept active until the last colliding packet has been solved or the SIC fails. To get an idea on the benefits brought by the inclusion of a NOMA scheme, in Fig. 7(b), the PER of a NOMA-powered SCM scheme is reported in comparison with a NOMA-based GFRA. The NOMA scheme considered is power-based in which a packet is considered decoded if the SINR is higher than the threshold $\Gamma = 4\,\mathrm{dB}$ [14]. The system parameters are the same as those in Fig. 6b in free-space condition. As expected, NOMA has a similar impact on the performance improvement in both schemes, being the SCM superior thanks to its more favorable link budget at high frequencies, as investigated in Section VII-A.

C. SCM vs BackCom Solutions

Metasurface-based BackCom communications have several similarities with our SCM-based scheme, but also profound

differences. Both are based on the backscatter modulation of a source RF signal, then they are characterized by the same two-way link budget and, in principle, by similar performance provided that the metasurface in the BackCom system is optimally configured and the AP has obtained a good estimate of the CSI [22]. The main difference relies on the fact that, to configure the metasurface, the CSI of the MIMO cascade channel must be estimated, and this typically takes a time proportional to the number of antenna elements [42]. Moreover, according to the estimated CSI, the AP must configure the metasurface in order to realize a suitable beamforming back to the AP which requires a dedicated control channel as well as additional complexity and energy consumption at the sensor. On the other hand, BackCom allows for multi-layer MIMO in case multiple sensors are co-located in the same metasurface, whereas our scheme realizes a single-layer MIMO (i.e., a single data stream). In summary, current BackCom schemes are not well suited for GFRA using short packets and low-complexity sensors, especially in dynamic scenarios.

D. Complexity and Scalability Considerations

From the computational complexity point of view, the Scouting Task is primarily driven by the orthogonalization operation in (15), which exhibits a complexity of $\mathcal{O}(NV)$, where N is the number of the AP's antennas and V represents the number of sensors transmitting simultaneously. Conversely, the complexity of the Communication Task is $\mathcal{O}(N)$, involving the computation of the decision variable. With V active Communication Tasks, the overall complexity remains at $\mathcal{O}(NV)$. Both the Scouting and Communication Tasks involve elementary operations whose number is proportional to the number N of antennas at the AP but not to the number of cells M at the SCM. Therefore, M can be considered as a useful degree of freedom that can be exploited to improve the link budget, and hence the $\mathsf{SNR}^{(\mathrm{boot})}$, without any drawback in terms of algorithm's complexity. Obviously, the complexity would significantly increase if a NOMA scheme is employed to improve the performance. Nevertheless, such an increase is the same one would obtain in conventional NOMA-based GFRA solutions.

In terms of scalability with the number of sensors, our scheme is not different from conventional multi-user MIMO systems. In particular, scalability can be addressed in two ways. Firstly, by increasing the number of antennas, resulting in narrower beams and more favorable propagation (massive MIMO). This reduces interference issues and allows for targeting a larger number of devices. Secondly, when the number of antennas is fixed, leveraging NOMA techniques to discriminate between users interfering with each other, as discussed before. As already mentioned, the key advantage of our solution compared to conventional multi-user MIMO systems is that the sensor node does not require any dedicated circuitry (such as RF chains, DACs, phase shifters, etc.) or signal processing capability (e.g., for CSI estimation) to perform beamforming.

VIII. Conclusion

In this paper, we have proposed the adoption of self-conjugating metasurfaces (SCMs) to realize low-complexity MIMO GFRA communications by leveraging retro-directive backscattering. Thanks to the iterative algorithm introduced in this paper, inspired by the Power Method, the AP can estimate the optimal beamforming vector for the AP-sensor round-trip channel and hence establish the optimal single-layer MIMO communication. Numerical results demonstrate that MIMO communications can be established after just a few iterations, with μs-level setup time, and no jitter, even using very large arrays and in the presence of realistic multipath channels. This scheme is particularly attractive in those applications envisioned for 6G, such as IIoT, where MIMO links must be established with reduced overhead and low latency to counteract the path loss at high frequencies. At the same time, it supports extremely low-complexity and low-energy consumption sensors transmitting short packets in a grant-free manner.

References

[1] S. R. Pokhrel et al., "Towards enabling critical mMTC: A review of URLLC within mMTC," *IEEE Access*, vol. 8, pp. 131796–131813, 2020.

[2] H. Viswanathan and P. E. Mogensen, "Communications in the 6G era," *IEEE Access*, vol. 8, pp. 57063–57074, 2020.

[3] Z. Wan, Z. Gao, M. Di Renzo, and L. Hanzo, "The road to industry 4.0 and beyond: A communications-, information-, and operation technology collaboration perspective," *IEEE Netw.*, vol. 36, no. 6, pp. 157–164, Dec. 2022.

[4] X. Chen et al., "Massive access for 5G and beyond," *IEEE J. Select. Areas Commun.*, vol. 39, no. 3, pp. 615–637, Mar. 2021.

[5] L. Liu and W. Yu, "Massive connectivity with massive MIMO—Part-I: Device activity detection and channel estimation," *IEEE Trans. Signal Process.*, vol. 66, no. 11, pp. 2933–2946, Jun. 2018.

[6] L. Liu et al., "Sparse signal processing for grant-free massive connectivity: A future paradigm for random access protocols in the Internet of Things," *IEEE Signal Process. Mag.*, vol. 35, no. 5, pp. 88–99, Sep. 2018.

[7] E. Paolini, C. Stefanovic, G. Liva, and P. Popovski, "Coded random access: Applying codes on graphs to design random access protocols," *IEEE Commun. Mag.*, vol. 53, no. 6, pp. 144–150, Jun. 2015.

[8] L. Yang et al., "Grant-free transmission by LDPC matrix mapping and integrated cover-MPA detector," 2022, *arXiv:2207.00272*.

[9] L. Valentini, M. Chiani, and E. Paolini, "Interference cancellation algorithms for grant-free multiple access with massive MIMO," *IEEE Trans. Wireless Commun.*, vol. 71, no. 8, pp. 4665–4677, Aug. 2023.

[10] J. Ding, D. Qu, H. Jiang, and T. Jiang, "Success probability of grant-free random access with massive MIMO," *IEEE Internet Things J.*, vol. 6, no. 1, pp. 506–516, Feb. 2019.

[11] J. Choi, "An approach to preamble collision reduction in grant-free random access with massive MIMO," *IEEE Trans. Wireless Commun.*, vol. 20, no. 3, pp. 1557–1566, Mar. 2021.

[12] M. B. Shahab, R. Abbas, M. Shirvanimoghaddam, and S. J. Johnson, "Grant-free non-orthogonal multiple access for IoT: A survey," *IEEE Commun. Surveys Tuts.*, vol. 22, no. 3, pp. 1805–1838, 3rd Quart., 2020.

[13] C. G. Kang, A. T. Abebe, and J. Choi, "NOMA-based grant-free massive access for latency-critical Internet of Things: A scalable and reliable framework," *IEEE Internet Things Mag.*, vol. 6, no. 3, pp. 12–18, Sep. 2023.

[14] J. Choi, "NOMA-based random access with multichannel ALOHA," *IEEE J. Select. Areas Commun.*, vol. 35, no. 12, pp. 2736–2743, Dec. 2017.

[15] W. Hao et al., "Robust design for intelligent reflecting surface-assisted MIMO-OFDMA terahertz IoT networks," *IEEE Internet Things J.*, vol. 8, no. 16, pp. 13052–13064, Aug. 2021.

[16] Z. Liu, J. Liu, Y. Zeng, and J. Ma, "Covert wireless communication in IoT network: From AWGN channel to THz band," *IEEE Internet Things J.*, vol. 7, no. 4, pp. 3378–3388, Apr. 2020.

[17] S. Cavallero et al., "Terahertz networks for future Industrial Internet of Things," *ITU J. Future Evolv. Technol.*, vol. 4, no. 1, pp. 196–208, Mar. 2023.
[18] S. Cavallero, K. Qirjako, R. Verdone, and C. Buratti, "A multi-hop industrial IoT network at THz bands using contention-based access," in *Proc. IEEE 34th Annu. Int. Symp. Pers., Indoor Mobile Radio Commun. (PIMRC)*, 2023, pp. 1–6.
[19] M. Giordani, M. Mezzavilla, and M. Zorzi, "Initial access in 5G mmWave cellular networks," *IEEE Commun. Mag.*, vol. 54, no. 11, pp. 40–47, Nov. 2016.
[20] J. Hu et al., "Meta-IoT: Simultaneous sensing and transmission by meta-material sensor based Internet of Things," *IEEE Trans. Wireless Commun.*, vol. 21, no. 8, pp. 6048–6063, Aug. 2022.
[21] H. Ding et al., "Symbiotic ambient backscatter systems: Outage behavior and Ergodic capacity," *IEEE Internet Things J.*, vol. 9, no. 23, pp. 23670–23690, Dec. 2022.
[22] Y.-C. Liang et al., "Backscatter communication assisted by reconfigurable intelligent surfaces," *Proc. IEEE*, vol. 110, no. 9, pp. 1339–1357, Sep. 2022.
[23] D. Dardari et al., "Ultrawide bandwidth RFID: The next generation?" *Proc. IEEE*, vol. 98, no. 9, pp. 1570–1582, Sep. 2010.
[24] J.-P. Niu and G. Y. Li, "An overview on backscatter communications," *J. Commun. Inf. Netw.*, vol. 4, no. 2, pp. 1–14, 2019.
[25] R. Miyamoto and T. Itoh, "Retrodirective arrays for wireless communications," *IEEE Microw. Mag.*, vol. 3, no. 1, pp. 71–79, Mar. 2002.
[26] D. Dardari, M. Lotti, N. Decarli, and G. Pasolini, "Establishing multi-user MIMO communications automatically using retrodirective arrays," *IEEE Open J. Commun. Soc.*, vol. 4, pp. 1396–1416, 2023.
[27] J.-F. Bousquet, S. Magierowski, and G. G. Messier, "A 4-GHz active scatterer in 130-nm CMOS for phase sweep amplify-and-forward," *IEEE Trans. Circuits Syst. I*, vol. 59, no. 3, pp. 529–540, Mar. 2012.
[28] K. K. Kishor and S. V. Hum, "An amplifying reconfigurable reflectarray antenna," *IEEE Trans. Antennas Propag.*, vol. 60, no. 1, pp. 197–205, Jan. 2012.
[29] C. Allen, K. Leong, and T. Itoh, "A negative reflective/refractive 'meta-interface' using a bi-directional phase-conjugating array," in *Proc. IEEE MTT-S Int. Microw. Symp. Dig.*, 2003, pp. 1875–1878.
[30] E. Sharp and M. Diab, "Van Atta reflector array," *IRE Trans. Antennas Propagat.*, vol. 8, no. 4, pp. 436–438, Jul. 1960.
[31] M. Kalaagi and D. Seetharamdoo, "Fano resonance based multiple angle retrodirective metasuface," in *Proc. 14th Eur. Conf. Antennas Propagat. (EuCAP)*, 2020 pp. 1–4.
[32] G. Alexandropoulos et al., "RIS-enabled smart wireless environments: Deployment scenarios, network architecture, bandwidth and area of influence," *J. Wireless Com Netw.*, vol. 103, pp. 1–38, Oct. 2023.
[33] H. Meyr, M. Moeneclaey, and S. A. Fechtel, *Digital Communication Receivers—Synchronization, Channel Estimation, and Signal Processing* (Wiley series in Telecommunications and Signal Processing). Hoboken, NJ, USA: Wiley, 1997.
[34] D. Tse and P. Viswanath, *Fundamentals of Wireless Communication*. New York, NY, USA: Cambridge Univ. Press, 2005.
[35] A.-S. Bana, G. Xu, E. D. Carvalho, and P. Popovski, "Ultra reliable low latency communications in massive multi-antenna systems," in *Proc. 52nd Asilomar Conf. Signals, Syst., Comput.*, 2018, pp. 188–192.
[36] G. H. Golub and H. A. van der Vorst, "Eigenvalue computation in the 20th century," *J. Comput. Appl. Math.*, vol. 123, no. 1, pp. 35–65, 2000.
[37] N. Decarli and D. Dardari, "Communication modes with large intelligent surfaces in the near field," *IEEE Access*, vol. 9, pp. 165648–165666, 2021.
[38] E. Björnson, J. Hoydis, and L. Sanguinetti, "Massive MIMO networks: Spectral, energy, and hardware efficiency," *Found. Trends Signal Process.*, vol. 11, nos. 3–4, pp. 154–655, 2017, doi: 10.1561/2000000093.
[39] X. Wu and D. Liu, "Novel insight into multi-user channels with multi-antenna users," *IEEE Commun. Lett.*, vol. 21, no. 9, pp. 1961–1964, Sep. 2017.
[40] T. Dahl, N. Christophersen, and D. Gesbert, "Blind MIMO eigenmode transmission based on the algebraic power method," *IEEE Trans. Signal Process.*, vol. 52, no. 9, pp. 2424–2431, Sep. 2004.
[41] "Study on channel model for frequencies from 0.5 to 100 GHz; (Release 16), Version 16.1.0," 3GPP, Sophia Antipolis, France, Rep. TR 38.901, 2019.
[42] T. L. Jensen and E. De Carvalho, "An optimal channel estimation scheme for intelligent reflecting surfaces based on a minimum variance unbiased estimator," in *Proc. IEEE Int. Conf. Acoust., Speech Signal Process.*, 2020, pp. 5000–5004.

Davide Dardari (Senior Member, IEEE) is a Full Professor with the University of Bologna, Italy. He has been a Research Affiliate with the Massachusetts Institute of Technology, USA. His interests are in wireless communications, localization techniques, smart radio environments, and distributed signal processing.

Prof. Dardari was received the IEEE Aerospace and Electronic Systems Society's M. Barry Carlton Award in 2011 and the IEEE Communications Society Fred W. Ellersick Prize in 2012. He was the Chair of the *Radio Communications Committee* and a Distinguished Lecturer from 2018 to 2019 of the IEEE Communications Society. He served as an Editor for the IEEE TRANSACTIONS ON WIRELESS COMMUNICATIONS from 2006 to 2012. He is currently a Senior Member of an Editorial Board of IEEE SIGNAL PROCESSING MAGAZINE.

Marina Lotti (Graduate Student Member, IEEE) received the B.S. and M.S. (cum laude) degrees in electronics and telecommunication engineering from the University of Bologna, Italy, in 2017 and 2020, respectively, where she is currently pursuing the Ph.D. degree with Smart Radio Environments Exploiting Reconfigurable Intelligent Surfaces. From 2020 to 2021, she was a Research Engineer with CEA-LETI, France, working on channel characterizations in the subTHz frequency range and radar measurements for localization and mapping purposes.

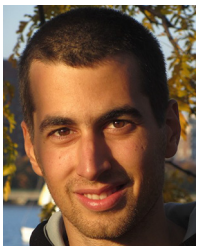

Nicolò Decarli (Member, IEEE) received the Ph.D. degree in electronics, telecommunications, and information technologies from the University of Bologna, Italy, in 2013. In 2012, he was a Visiting Student with the Wireless Communication and Network Sciences Laboratory, Massachusetts Institute of Technology, Cambridge, MA, USA. He is currently a Researcher with the Institute of Electronics, Computer, and Telecommunication Engineering, National Research Council, Italy. His research interests include wireless communication theory, integration of communication, localization and sensing, and smart radio environments.

Gianni Pasolini (Member, IEEE) received the M.Sc. degree in telecommunications engineering and the Ph.D. degree in electronic engineering and computer science from the University of Bologna, Italy, in 1999 and 2003, respectively, where He is currently an Associate Professor with the Department of Electrical, Electronic and Information Engineering and he has been teaching various courses in the field of telecommunications since 2003. His research interests encompass wireless communication systems, Internet of Things, digital signal processing, and THz communications. He was the recipient of the Best Paper Award at the 2023 IEEE International Conference on Communications. Throughout his career, he has actively participated in several European initiatives focused on wireless communications, including COST actions and Networks of Excellence. He serves as an Associate Editor for IEEE OPEN JOURNAL OF THE COMMUNICATIONS SOCIETY. He served as a member of the Organizing Committee for the 2018 IEEE International Symposium on Personal, Indoor and Mobile Radio Communications, the 2017 IEEE International Symposium on Wireless Communication Systems, and the 2011 IEEE International Conference on Ultra-Wideband. He is one of the Founding Member of the "National Laboratory of Wireless Communications–Wilab" of the National Inter-University Consortium for Telecommunications, Italy.

Open Access funding provided by 'Consiglio Nazionale delle Ricerche-CARI-CARE-ITALY' within the CRUI CARE Agreement